Weld pool shape identification by using Bezier surfaces

Duc Dung Doan, Franck Gabriel, Yvon Jarny, Philippe Le Masson

Weld Pool Shape Identification by Using Bezier Surfaces

DUC DUNG DOAN,[1] FRANCK GABRIEL,[1] YVON JARNY,[3] and PHILIPPE LE MASSON[1]

[1]Atomic Energy Agency, Saclay, France
[2]Polytech' Nantes Site de Chantrerie, University of Nantes, Nantes, France, and
[3]LIMATB, University of South Brittany, Lorient, France

This paper deals with the heat transfer analysis in a welding process: A method is developed to determine the shape of the three-dimensional (3-D) phase change front and to estimate the temperature field within the solid part of the work piece. The problem is formulated and solved as an inverse phase-change problem by using an optimization method. The direct problem is solved in the torch frame and so formulated as an Eulerian approach. The interface between the weld pool and the solid region is parameterized by Bezier surfaces. The most important feature of the presented approach is that the liquid–solid interface as well as the temperature distribution within the solid region can be obtained from additional temperature data available in the solid region, without considering heat transfer and fluid flow in a molten zone. The estimate of these thermal characteristics then allows a thermomechanical calculation of the welded joint (calculation of the deformations and residual stresses). The validity of the numerical solution of the inverse problem is checked by comparing the results with the direct solution of the problem.

INTRODUCTION

Welding is a complex process that involves many parameters that may have important influences on the final solidification structure and the properties of the welded joint [1]. During the welding process, the edge of two pieces of metal are melted and fused together. This is done using an intense local energy source. Transmitted energy causes the fusion of metal, as well as the creation of a molten pool usually referred to as a weld pool. It is important to be able to control the size and shape of the weld pool [2]. It must be small enough to be manageable and minimize energy consumption but large enough to bond the two pieces properly

Studies that deal with the inverse technique for the analysis of melting and solidification processes are limited. Earlier efforts have focused on a one-dimensional problem [3–5]. The literature includes the two-dimensional (2-D) stationary arc welding problem in which Hsu uses transient temperature data from thermocouples imbedded in the solid region to determine through a Newton–Raphson interpolation procedure the transient position of the liquid–solid interface and the transient temperature distribution in the solid region [6]. Later, it includes the two-dimensional design problem [7–8] and the two-dimensional inverse geometry problem in continuous casting of metals [9]. Recently, Doan et al. have developed an original method to identify the position and the shape of a 2-D melting pool using the parameterization by Bezier splines [10–14].

This work focuses on the application of the inverse technique and Bezier surfaces for identifying the location of the three-dimensional (3-D) liquid–solid interface, as well as its application with Bezier splines in the 2-D case. Furthermore, it can be noted that in quasi-steady state, the determination of the heat flux crossing this interface results directly from the knowledge of both the front location and the temperature field within the solid region.

PROBLEM STATEMENT

The Welding Processes

The phase-change phenomenon is considered in the following experimental conditions (Figure 1). A welding arc having

Address correspondence to Professor Philippe Le Masson, LIMATB University of South Brittany, UEB, Rue de Saint Maudé, BP 92116 56321, Lorient Cedex, France. E-mail: philippe.le-masson@univ-ubs.fr

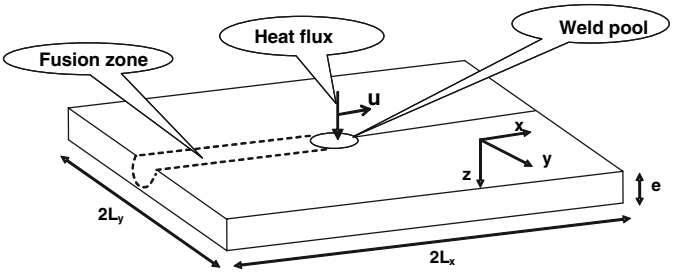

Figure 1 Schematic diagram of welding process.

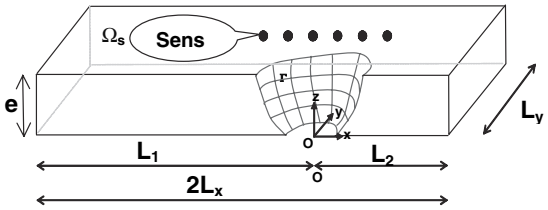

Figure 2 Schematic of spatial domain.

a power of sufficient intensity moves with a constant velocity (axis x) and strikes the edge of two metal plates. A weld pool is formed and moves at the same velocity as the welding arc.

The mathematical representation of the problem includes the following physical processes and other general assumptions and conditions:

1. The heat transfer between two plates during the welding process when the welding torch moves with a constant velocity is unsteady in a fixed coordinate system. A quasi-steady-state problem can be achieved in a coordinate system that moves with the heat source. Thus, a moving coordinate system is used for the analysis of the inverse problem. This means that the size of the weld pool under the welding arc is constant while the material enters and leaves the computational domain.
2. In quasi-steady state, to obtain the shape of the weld pool and the temperature field in the solid domain, we formulate and solve the heat conduction problem within the solid region by considering the melting temperature as the imposed temperature at the liquid–solid interface.
3. The Bezier surface with its control points is used to define the position of the liquid–solid interface. In this work, this assumption is used in order to form the initial position of the liquid–solid interface and to create a numerical experiment, i.e., the temperature data at the points of measurement located within the solid region. The location of the sensors is constant with respect to the moving coordinate.

We first analyze the mathematical formulation of the general 3-D problem and its numerical solution with Bezier surfaces, and then we apply the method in a 2-D case.

Modeling Equations

3-D Cases (Figure 2)

The modeling equations that determine the temperature field within the solid region consist of the energy equation (1) with a moving heat source along the x axis, together with adiabatic conditions on the boundaries and a symmetric condition (2), the condition at the top and the bottom of the work piece [Eqs. (3) and (4)], the imposed temperature on the boundary at $x = +L_2$, and the specification of the melting temperature along the phase-change front (5).

$$\rho_s c_s u \frac{\partial T_s(x, y, z)}{\partial x} = \nabla.\,[\lambda_s \nabla T_s(x, y, z)] \qquad (x, y, z) \in \Omega_S \tag{1}$$

$$\frac{\partial T_s}{\partial y} = 0 \; at \; y = L_y; \frac{\partial T_s}{\partial x} = 0 \; at \; x = -L_1 \; and$$

$$\frac{\partial T_s}{\partial y} = 0 \; at \; y = 0 \tag{2}$$

$$-\lambda_s \frac{\partial T\,(x, y, z_0)}{\partial z} + hT(x, y, z_0) = hT_e \; at \; z = z_0 = 0 \tag{3}$$

$$\lambda_s \frac{\partial T\left(x, y, z_{ep}\right)}{\partial z} + hT(x, y, z_{ep}) = hT_e \; at \; z = z_{ep} = e \tag{4}$$

$$T = T_{imp} \;\; at \;\; x = +L_2\,, \;\; T\,(x, y, z) = T_f \;\; at \;\; (x, y, z) \in \Gamma \tag{5}$$

The shape Γ of the isothermal phase change front is unknown. Considering a heat flux balance equation to determine this shape is nonpracticable because no experimental data are available to characterize the heat flux distribution lost by the weld pool through this front. Therefore the shape of the front will be determined using an inverse approach, which needs additional data given by the temperature measurements at M points located in the solid region:

$$T\,(x_m, y_m, z_m) = Y^m m = 1, 2, \ldots, M(x, y, z) \in \Omega_s \tag{6}$$

Hence the inverse problem, considered of interest here, aims for the shape Γ identification of the phase change front and the estimation of the temperature field within the solid part $\Omega_s$of the work piece for the modeling Eqs. (1)–(6). The main difficulty in this kind of problem is its ill-posed nature. That is why the measurement sensor number should be appropriate to make an overdetermined problem, or at least equal to the number of design variables. Thus, in general, inverse analysis leads to optimization procedures of an objective function S(X) of

the least-squares type built with $T(x_m, y_m, z_m; \Gamma)$, the predicted temperatures by the modeling Eqs. (1)–(5), Γ being fixed, and the measured temperatures, as in Eq. (6). The inverse phase change problem is formulated as an optimization problem; it consists of finding Γ that minimizes:

$$S(\Gamma) = \frac{1}{M}\sum_{m=1}^{M}\left(T(x_m, y_m, z_m; \Gamma) - Y^m\right)^2 \tag{7}$$

Then the inverse analysis is performed without solving heat transfer and fluid flow equations in the liquid region. The idea of the iterative algorithm is as follows:

- Step 1: Choose an initial guess of the shape $\Gamma$and its parameterization by Bezier splines (see next section).
- Step 2: Compute the sensitivity of the predicted temperature at the sensor locations with respect to the vector parameter X of Bezier splines, defined by the coordinates of the control points.
- Step 3: Use the Levenberg Marquardt algorithm [15] to correct the vector parameter X.
- Step 4: Repeat the procedure until convergence is achieved.

Modeling of phase-change processes requires smooth curves representing phase-change fronts. Al-Khadily [7] describes the phase-change boundary with a two-dimensional coordinate system assumed in the molten zone. Each point at the phase change boundary is located by its radial and angular coordinates, i.e., radial distance from the keyhole center and the angular direction. Since the interface location is just a guess, the obtained temperature profile through the work piece will differ from the exact. The exact location of the liquid–solid interface, as well as the temperature profile, is found by use of the prediction-correction method. Choice of the number of nodes to form the interface plays a major role in obtaining accurate and efficient solution of the inverse problem. However, when the shape of the phase-change fronts is complex this number of nodes is important, i.e., more measurement sensors are needed. As noticed before, the ill-posed nature of all inverse problems requires making them overdetermined by performing an appropriate number of measurements. On the other hand, it is very important to limit the number of sensors because of commonly known difficulties with data acquisition. Furthermore, each measurement introduces not only variable information but also some noise. Application of Bezier surfaces permits us to parameterize the phase change front using a smaller number of parameters and, consequently, reduce the number of sensors.

2-D Application (Figure 3)

Formulation of the inverse problem. When the thickness e of the piece is weak enough, the modeling Eqs. (1)–(5), which determine the temperature field within the solid region, reduce to the following forms:

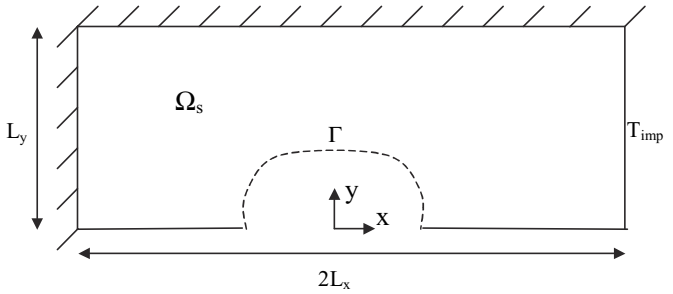

Figure 3 Schematic of the 2-D spatial domain.

$$\rho_s c_s u \frac{\partial T_s(x, y)}{\partial x} = \nabla.\left[\lambda_s \nabla T_s(x, y)\right]$$

$$-\frac{hp}{S}\left(T_s - T_{imp}\right)(x, y) \in \Omega_s \tag{8}$$

$$\frac{\partial T_s}{\partial y} = 0 \text{ at } y = L_y, \tag{9a}$$

$$\frac{\partial T_s}{\partial x} = 0 \text{ at } x = -L_x \tag{9b}$$

$$\frac{\partial u}{\partial y} = 0, \frac{\partial T_s}{\partial y} = 0 \text{ at } y = 0 \tag{9c}$$

$$T_s = T_{imp} \text{ at } x = +L_x, T_s(x, y) = T_f \text{ at } (x, y) \in \Gamma \tag{10}$$

The second term in the right-hand side of Eq. (8) is used to define the heat lost by convection and by radiation from the upper and the lower surfaces of the work piece, where $p = 2\left(2L_y + e\right)$ and $S = 2L_y \times e$ are the perimeter and the section area of the work piece.

Additional data are given by the temperature measurements at M points located in the solid region:

$$T(x_m, y_m) = Y^m m = 1, 2, \ldots, M(x, y) \in \Omega_s m \tag{11}$$

The inverse phase change problem is formulated, as in the 3-D cases, as an optimization problem; it consists in finding Γ that minimizes

$$S(\Gamma) = \frac{1}{M}\sum_{m=1}^{M}\left(T(x_m, y_m; \Gamma) - Y^m\right)^2 \tag{12}$$

In order to optimally identify and represent the weld pool shape, it is parameterized with the Bezier surfaces in 3-D cases and with Bezier splines in 2-D cases.

***Parameterization of the Front* Γ**

Bezier Surfaces

Generally, the Bezier surface is formulated as follows:

$$P(u,v)=\sum_{i=0}^{m}\sum_{j=0}^{n}B_i^m(u)B_j^n(v)P_{ij}\ \text{with}\ u\in[0,1],\ v\in[0,1]$$

$$B_i^m(u)=\frac{m!}{i!\,(m-i)!}u^i\,(1-u)^{m-i}$$

$$B_j^n(v)=\frac{n!}{j!\,(n-j)!}v^j\,(1-v)^{n-j} \tag{13}$$

where *P(u,v)* stands for any point on the Bezier surface, P_{ij} is the control point, $m \times n$ is the degree of Bezier surface, $N=(m+1)\times(n+1)$ is the number of control point, u and v vary in the range [0, 1], and $B_i^n(u)$, $B_i^n(v)$ are the Bernstein polynomials.

The majority of weld pool interfaces can be represented by a cubic Bezier surface (with $m=2,\ n=3$). Such curves applied in the 3-D fully penetration weld pool problem are based on 12 control points P_0, P_1, P_2, …, P_{12} (Figure 4) as presented in the following formulation:

$$\begin{aligned}P(u,v)=&\sum_{i=0}^{2}\sum_{J=0}^{3}P_{ij}\frac{2!}{i!\,(2-i)!}u^i\,(1-u)^i\\&\times\frac{3!}{j!\,(3-j)!}v^j\,(1-v)^{3-j}=P_{00}\,(1-u)^2\,(1-v)^3\\&+P_{01}\,(1-u)^2\,3v\,(1-v)^2+P_{02}\,(1-u)^2\\&\times 3v^2\,(1-v)+P_{03}\,(1-u)^2\,v^3\\&+P_{10}2u\,(1-u)\,(1-v)^3+P_{11}2u\,(1-u)\\&\times 3v\,(1-v)^2\end{aligned}$$

$$\text{with}\qquad u\in[0,1];\ v\in[0,1] \tag{14}$$

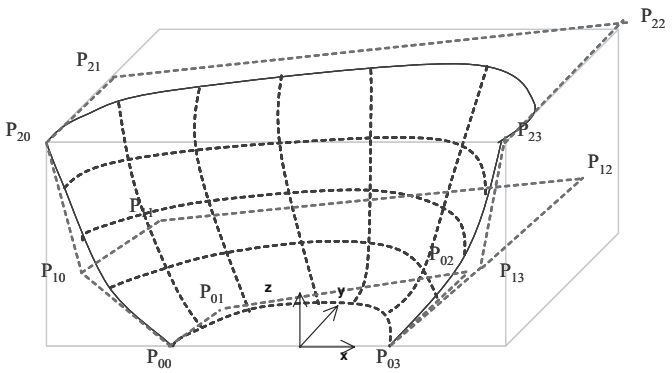

Figure 4 Surface of degree (2 × 3) with its 12 control points.

This means that the shape of the interface Γ is described by 12 control points (i.e., 36 coordinates in the 3-D case). The proposed approach has a number of important advantages. First, the application of Bezier surface of degree (2 × 3) ensures smoothness of the phase change front. The next very important advantage is that this application permits to limit the size of the vector parameter X to be identified.

In practice, some coordinates of the Bezier control points are defined by additional conditions resulting from the physical nature of the problem. In the case studied here we have

$$P_{00y}=P_{10y}=P_{20y}=P_{03y}=P_{13y}=P_{23y}=0.$$

On the other hand, by using the symmetry condition, we have $P_{21x}=P_{20x}$, $P_{22x}=P_{23x}$, $P_{01x}=P_{00x}$, $P_{02x}=P_{03x}$, $P_{11x}=P_{10x}$, $P_{12x}=P_{13x}$. We impose $P_{10z}=P_{11z}=P_{12z}=P_{13z}$.

Finally, the size of the vector parameter X is limited to $\dim(X)=12$ with

$$\begin{aligned}X=\big[&P_{00x},\,P_{03x},\,P_{01y},\,P_{02y},\,P_{10x},\\&\times\ P_{13x},\,P_{11y},\,P_{12y},\,P_{20x},\,P_{23x},\,P_{21y},\,P_{22y}\big].\end{aligned}$$

Bezier Splines

Generally, the Bezier splines are formulated as follows:

$$P(t)=\sum_{i=0}^{n}B_i^n(t)P_i$$

$$B_i^n(t)=C_i^n u^i(1-t)^{n-i},\ C_i^n=\frac{n!}{i!(n-i)!};i=1,..n$$

$$N=n+1 \tag{15}$$

where *P(t)* stands for any point on the Bezier spline, P_i is the control point, n is the degree of Bezier spline, $N=n+1$ is the number of control point, t varies in the range [0, 1], and $B_i^n(t)$ is the Bernstein polynomial.

The majority of weld pool interfaces can be represented by cubic Bezier splines (with $n=3$). Such curves are based on four control points P_0, P_1, P_2, and P_3 (Figure 5) as presented in the

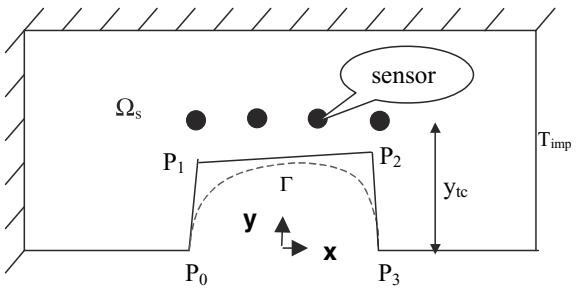

Figure 5 Schematic of the spatial domain.

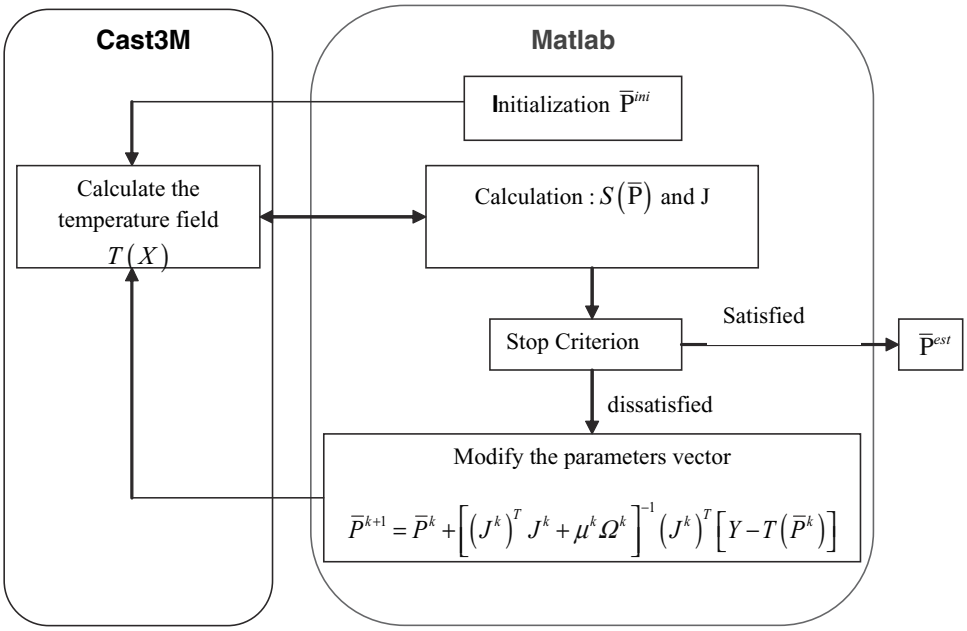

Figure 6 Coupling the Matlab and Cast3M software.

following formulation:

$$P(t) = (1-t)^3 P_0 + 3(1-t)^2 t P_1 + 3(1-t)t^2 P_2 + t^3 P_3 \quad 0 \le t \le 1 \tag{16}$$

This means that the shape of the interface Γ is described by four control points (i.e., eight coordinates in the 2-D case). In practice, some coordinates of the Bezier control points are defined by additional conditions resulting from the physical nature of the problem. In the case studied here four coordinates are assumed to be given; then the size of the vector parameter $X = \left[P_{0x}, P_{1y}, P_{2y}, P_{3x}\right]$is limited to four.

The next step of the study consists in developing some numerical experiments in order to validate the inverse approach. We first validate the 2-D case and then the 3-D case. The optimization computations are numerically performed by using the Cast3M and Matlab software as presented in the Figure 6.

NUMERICAL RESULTS

The solution of the inverse problem is considered with simulated data. Several numerical experiments have been performed in order to:

Make the solution and convergence limits independent on computational parameters.
Choose a suitable number of sensors and their locations and simplify the experimental design procedure.

The parameters to be identified are the control point's coordinates and the overheat transfer coefficient h.

The sensitivity analysis [14] is detailed in order to analyze the influence of the sensor locations as well as the influence of the parameters supposed to be known, i.e., λ_s, ρ_s, c, u, T_e, and y_{TC}. It was observed that the computed solutions are very sensitive to the errors on these last parameters, which can provide significant bias in the result of the identification problem. However, the sensitivity to the coefficient h remains very weak, so we choose to use a constant value coming from Goldak [16].

Thin Plate Case (2-D Application)

Numerical Experiment

For example, the temperature field $T(x, y; \Gamma)$ plotted in Figure 7 was obtained by solving the modeling Eqs. (8)–(11) with a finite-element approximation and the following

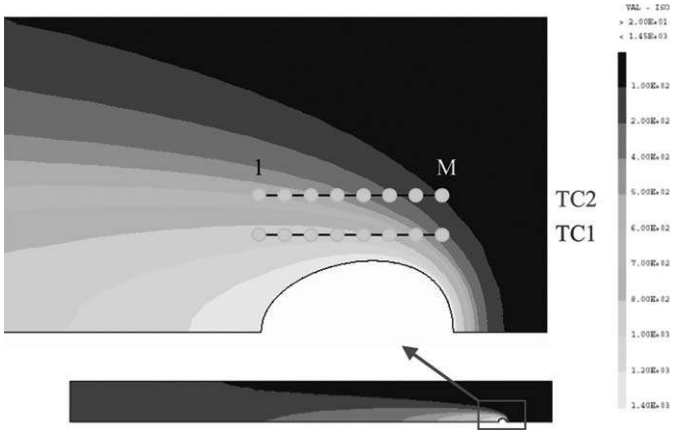

Figure 7 Temperature field in the solid region given by numerical experiment.

numerical values:

$$L_x = 30\ cm,\ L_y = 5\ cm,\ \rho_s = 7200\ \mathrm{kg/m^3},\ \rho_s c_p = 400000\ J/m^3K,\ \lambda_s = 50\ W/mK,$$

$$T_f = 1450^\circ C,\ T_{imp} = 20^\circ C,\ u = 10\ mm/s,$$

$$T_{ref} = 300\ K;\ \varepsilon = 0.9$$

$$h = 23.45 \times \varepsilon \left(\frac{T}{T_{ref}}\right)^{1.61} \quad (W/m^2K)$$

The shape of the front is parameterized by the four following control points $P_0^{\exp}(-0.0067,\ 0)$, $P_1^{\exp}(-0.0067,\ 0.00375)$, $P_2^{\exp}(0.0033,\ 0.006)$, and $P_3^{\exp}(0.0033,\ 0.)$,

The vector parameters to be found are

$$X^{\exp} = \left(P_{0x}^{\exp}, P_{1y}^{\exp}, P_{2y}^{\exp}, P_{3x}^{\exp}\right) = (-0.0067, 0.00375, 0.006, 0.0033).$$

Results and Discussion—Influence of the Choice of Initial Parameters X^{ini}

The optimization problem may have several local minima. The influence of the initial guess X^{ini} on the computed solution has to be investigated. The weld pool physical nature imposes some constraints on the initial parameter values, especially on the weld pool length $Long_{bain}$ and width Lar_{bain}: $Long_{bain} \geq Lar_{bain}$. Moreover, $Long_{bain} = (P_{3x} - P_{0x})$ and Lar_{bain} depends on P1y and P2y. That leads us to choose the initial parameters X^{ini} with four control points of a Bezier spline checking the ellipse equation curve $P(t) \equiv \frac{x^2}{a^2} + \frac{y^2}{b^2} = 1$ with $a > b$, as in Figure 8. In practice, $P_{2y} \geq P_{1y}$, and we consider then $P_{2y}^{ini} = P_{1y}^{ini}$. On the other hand, $b = Max[P_y(t)] = Max[(1-t)^3 P_{0y} + 3t(1-t)^2 P_{1y} + 3t^2(1-t)P_{2y} + t^3 P_{3y}]$; then $P_{0y} = P_{3y} = 0$ implies $b = Max[3t(1-t)^2 P_{1y} + 3t^2(1-t)P_{2y}]$, so the maximum value is at $t = 0,5$, and $b = \frac{3}{8}P_{1y} + \frac{3}{8}P_{2y}$. Therefore, the initial guess is chosen in order to check the following conditions:

$$\left.\begin{array}{l} P_{3x}^{ini} - P_{0x}^{ini} = 2a \text{ then } P_{3x}^{ini} = -P_{0x}^{ini} = a \\ \frac{3}{8}P_{1y}^{ini} + \frac{3}{8}P_{2y}^{ini} = b \text{ then } P_{1y}^{ini} = P_{2y}^{ini} = \frac{4}{3}b \\ a > b \end{array}\right\} \text{(A*)}$$

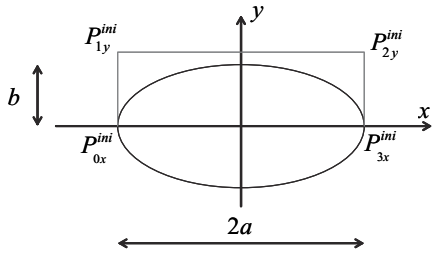

Figure 8 The choice of initial guess.

To facilitate the numerical procedure, the parameter coordinates are defined in the range [0, 1] by a simple transformation $P_{ik} = \|P_{ik}\| / \|P_{norm}\|$.

Here we have $P_{Ox} = \frac{\|P_{0x}\|}{0.008}$, $P_{1y} = \frac{\|P_{1y}\|}{0.007}$, $P_{2y} = \frac{\|P_{2y}\|}{0.007}$, $P_{3x} = \frac{\|P_{3x}\|}{0.008}$, so the vector parameter to be found is $X_{tr}^{\exp} = (0.838,\ 0.536,\ 0.857, 0.413)$.

The initial guess conditions (A*) become:

$$\left.\begin{array}{l} P_{3x}^{ini} = P_{0x}^{ini} = \frac{a}{0.008},\ \text{then } 0 \leq a \leq 0.008 \\ P_{1y}^{ini} = P_{2y}^{ini} = \frac{4}{3*0.007}b = \frac{4}{0.021}b \text{ then } 0 \leq b \leq \frac{0.021}{4} \\ a > b \end{array}\right\} \text{(A**)}$$

Several tests, with different initial parameter vector (Table 1), are carried out in order to analyze convergence for the case using $M = 100$ measurement data. The sensors are located at $y_{TC} = 7,0\ mm$ (Table 2), $y_{TC} = 6,0\ mm$ (Table 3) and $y_{TC} = 5,5\ mm$ (Table 4).

The estimation error is given by $\varepsilon^{est} = \|\Delta P\| / \|P\| = \sqrt{\sum \left(P_{ik}^{\exp} - P_{ik}^{cal}\right)^2} / \sqrt{\sum \left(P_{ik}^{\exp}\right)^2}$ and $T_{\max}$is the maximum measured temperature.

All these initializations lead to the exact solution. But the following results show the influence of the sensor locations on the convergence of the optimization algorithm: The more the sensors are close to the front, the more the measurements points are sensitive, i.e., the solution of the identification problem is better and the convergence is faster. In addition, it is better to choose the configuration number 5 or number 6 (Table 1) to initialize the calculation of optimization (Tables 2–4).

In conclusion, in the analysis of these tables, it is observed that the most favorable cases are those where the initial form is located within the exact form.

The parameter estimation in the favorable case number 6 with $y_{TC} = 5,5\ mm$ is presented in Figure 9. The exact front and the estimated one are plotted in Figure 10, as well as the difference between these two fronts in Figure 11. One can note that the maximum error is 35 μm for a weld pool length equal to 10 mm. The relative error is then lower than 1%. After the estimation of the weld pool shape Γ, knowing the temperature field within the solid part, one can calculate the heat flux crossing Γ, along the curvilinear X-coordinate (see Figure 12). It is noted that heat flow increases from 0.04 MW m^{-2} to 1.02 MW m^{-2} and reaches its maximum value at the head of the fusion front.

Table 1 Configuration between initial Γini (ini) and the exact front Γexp (exp)

Number	X^{ini} $\left(P_{0x}, P_{1y}, P_{2y}, P_{3x}\right)$	Comparison between initial Γini (ini) and the exact front Γexp (exp)
1	(0.9 0.8 0.8 0.9)	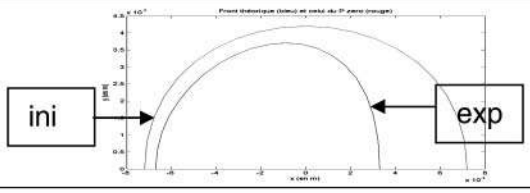
2	(0.4 0.8 0.8 0.4)	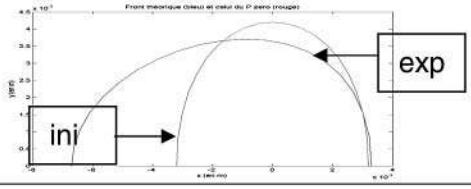
3	(0.25 0.6 0.6 0.25)	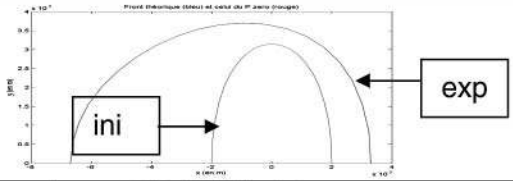
4	(0.8 0.4 0.4 0.8)	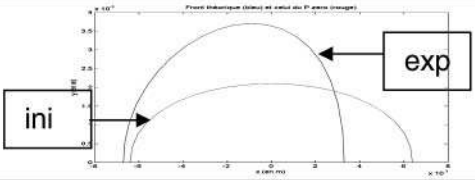
5	(0.2 0.4 0.4 0.2)	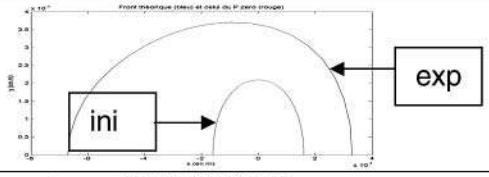
6	(0.2 0.2 0.2 0.2)	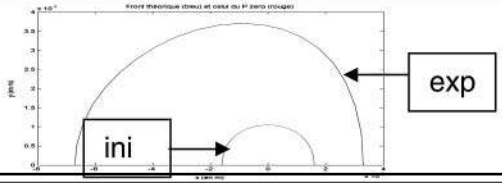

Table 2 Influence of the choice of initial guesses with $y_{TC} = 7,0\ mm$

Test number	$X^{ini}(P_{0x}, P_{1y}, P_{2y}, P_{3x})$	$\sqrt{S}$ (Eq. 12)	Iteration number	$\sqrt{S}/T_{\max}$ (%) ($T_{\max} = 7.3.31°C$)	ε^{est}(%)
1	(0.90.80.80.9)	3.00	24	0.42	22.20
2	(0.40.80.80.4)	9.43	18	1.34	20.50
3	(0.250.60.60.25)	1.35	20	0.19	1.27
4	(0.80.40.40.8)	4.67	33	0.66	10.98
5	(0.20.40.40.2)	2.38	28	0.34	14.20
6	(0.90.60.80.65)	1.6	25	0.22	8.60

Table 3 Influence of the choice of Initial guesses with $y_{TC} = 6,0\ mm$

Test number	$X^{\text{ini}}(P_{0x}, P_{1y}, P_{2y}, P_{3x})$	$\sqrt{S}$	Iteration number	$\sqrt{S}/T_{\max}$ (%) ($T_{\max} = 821.03^{\circ}C$)	ε^{est} (%)
1	(0.9 0.8 0.8 0.9)	16.68	25	2.03	17.70
2	(0.4 0.8 0.8 0.4)	2.90	22	0.35	17.80
3	(0.25 0.6 0.6 0.25)	2.32	40	0.28	13.90
4	(0.8 0.4 0.4 0.8)	8.09	39	0.99	12.40
5	(0.2 0.4 0.4 0.2)	1.37	25	0.17	2.00
6	(0.2 0.2 0.2 0.2)	0.53	24	0.06	1.16

Table 4 Influence of the choice of initial guesses with $y_{TC} = 5,5\ mm$

Test number	X^{ini} $(P_{0x}, P_{1y}, P_{2y}, P_{3x})$	$\sqrt{S}$	Iterations number	$\sqrt{S}/T_{\max}$ (%) $(T_{\max} = 909.24^{\circ C})$	ε^{est} (%)
1	(0.9 0.8 0.8 0.9)	2.26	42	0.25	4.06
2	(0.4 0.8 0.8 0.4)	1.87	34	0.21	5.78
3	(0.25 0.6 0.6 0.25)	1.52	30	0.17	2.83
4	(0.8 0.4 0.4 0.8)	1.44	28	0.16	4.33
5	(0.2 0.4 0.4 0.2)	1.75	16	0.19	6.45
6	(0.2 0.2 0.2 0.2)	1.54	26	0.17	1.20

Thick Plate (3-D Application)

In this section, we consider two kinds of weld pool shape identification: the partial penetration case and the full penetration case.

Full Penetration Case

We present here a case test representative of a TIG or MIG/MAG welding process configuration. The liquid/solid interface (fusion front) is parameterized by using a Bezier surface of degree 2×3 described previously. Applying the method of reduction of the parameters number presented previously, the

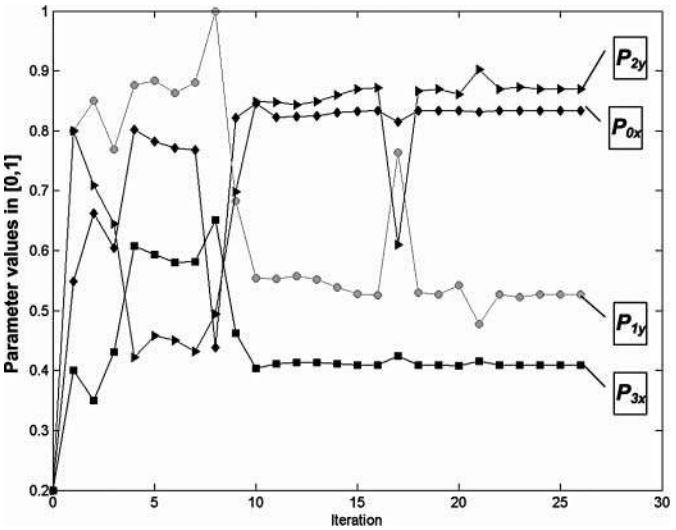

Figure 9 2-D numerical experiment—parameter estimation (test number 6 with $y_{TC} = 5,5\ mm$).

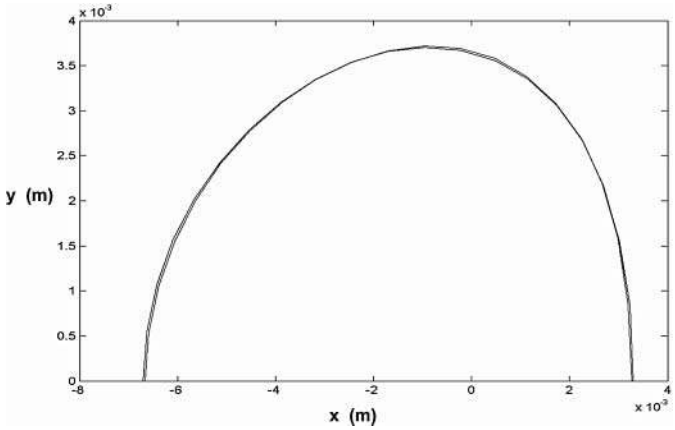

Figure 10 Comparison between the exact and estimated fronts (test number 6 with $y_{TC} = 5,5\ mm$).

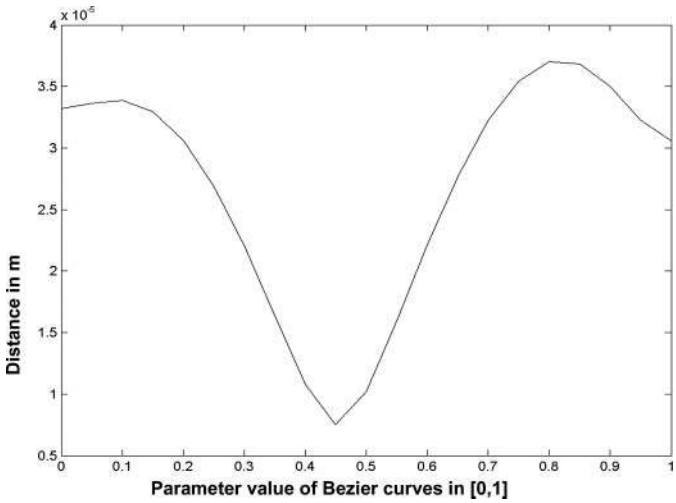

Figure 11 Error between the exact front and the estimated one.

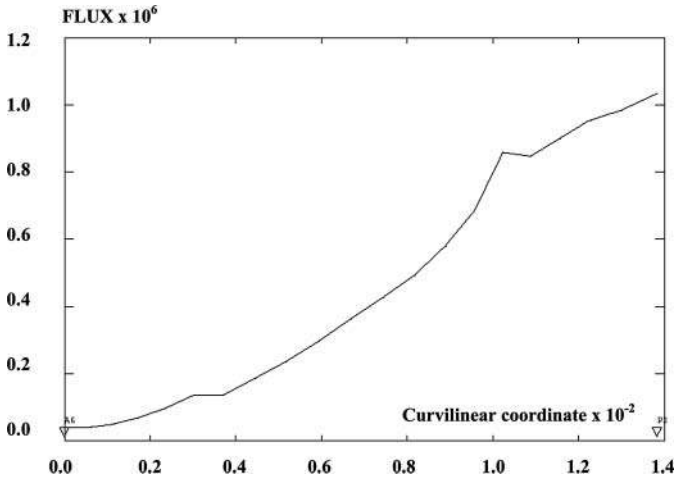

Figure 12 Heat flux crossing the fusion front according to curvilinear coordinate.

fusion front can be written as:

$$\Gamma = \Gamma\left(P_{00x}, P_{03x}, P_{01y}, P_{02y}, P_{10x}, P_{13x}, P_{11y}, \times P_{12y}, P_{20x}, P_{23x}, P_{21y}, P_{22y}\right)$$

The direct problem formulation is presented in Eqs. (1) to (7). The optimization problem consists in finding Γ by minimizing the difference between the measured and calculated temperatures. The identification problem in 3-D follows the same process as that of the 2-D problem.

3-D Numerical Experiment (Figures 13 and 14). The reference temperature field presented in Figures 15 and 16 is obtained using Cast 3M software with the following data: $h = 24.1 Wm^{-2}K^{-1}$, $L_y = 40\ mm$, $L_x = 300\ mm$, $e = 3\ mm$, $\rho_s c_p = 4000000\, J.m^{-3}.K^{-1}$, $\lambda_s = 50\, W.m^{-1}.K^1$, $T_f = 1450^\circ C$, $T_{imp} = 20^\circ C$, and $v_{torche} = 10\, mm.s^{-1}$. The shape of the front is defined by a Bezier surface with the following 12 control points: $P_{00}^{\exp}(-0.006\,00)$, $P_{01}^{\exp}(-0.006\,0.006\,0)$, $P_{02}^{\exp}(0.004\,0.006\,0)$, $P_{03}^{\exp}(0.004\,0\,0)$, $P_{10}^{\exp}(-0.0075\,0\,0.0015)$, $P_{11}^{\exp}(-0.0075\,0.006\,0.0015)$, $P_{12}^{\exp}(0.005\,0.009\,0.0015)$, $P_{13}^{\exp}(0.005\,0\,0.0015)$, $P_{20}^{\exp}(-0.009\,0\,0.003)$, $P_{21}^{\exp}(-0.009\,0.008\,0.003)$, $P_{22}^{\exp}(0.0060.010.003)$, and $P_{23}^{\exp}(0.00600.003)$.

The measurement points are on the top plane ($z = e$) and the bottom plane ($z = 0$) (Figure 13), respectively, at the distance y_{ed}, y_{ev} of the middle plane "*x0z*." With the molten zone being more developed on the top than on the bottom plane, we take $y_{ed} = 7,5\ mm > y_{ev} = 5,5\ mm$. The method also makes it possible to use measurement points located inside the plate.

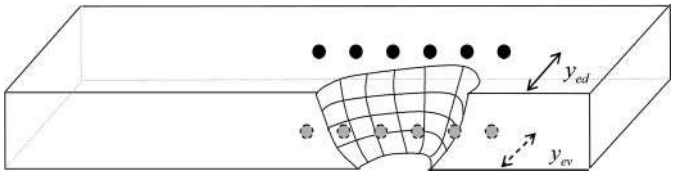

Figure 13 Sensors location.

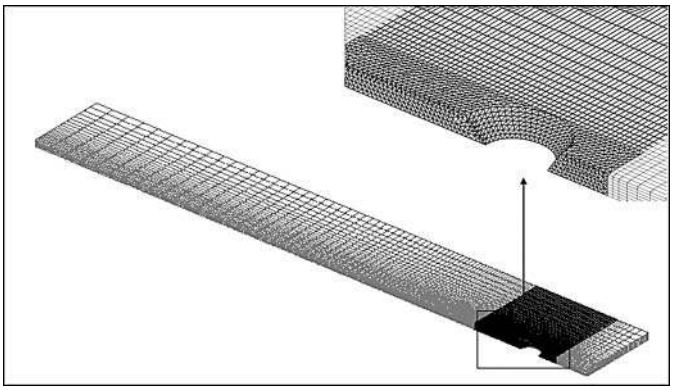

Figure 14 3-D mesh in the full penetration case.

Here, this information was not taken into account.

Results and Discussion—Influence of the Choice of Initial Parameters X^{ini}. Various initial parameters are checked in order to analyze convergence. The vector of the parameters to be estimated is:

$$X = \left[P_{00x}, P_{03x}, P_{01y}, P_{02y}, P_{10x}, P_{13x}, P_{11y}, \times P_{12y}, P_{20x}, P_{23x}, P_{21y}, P_{22y}\right]$$

$$X^{\exp} = [-0.006\,0.004\,0.006\,0.006 - 0.0075\,0.005\,0.006\,0.009 \\ -0.009\,0.006\,0.008\,0.01]$$

We apply the same technique concerning the choice of X^{ini} presented in the 2-D case. We thus start the optimization calculation with an initialization that satisfies the following conditions:

$$P_{23x} - P_{20x} = long_{bain}^{ed} > larg_{bain}^{ed}$$
$$P_{03x} - P_{00x} = long_{bain}^{ev} > larg_{bain}^{ev}$$

We choose a configuration for the initial parameters as follows (Figure 17):

$$\left.\begin{array}{l} P_{23x} = P_{13x} = P_{03x} = a; \quad P_{20x} = P_{10x} = P_{00x} = -a \\ P_{21y} = P_{22y} = P_{11y} = P_{12y} = P_{01y} = P_{02y} = \frac{4}{3}b \\ a > b \end{array}\right\} \text{(B*)}$$

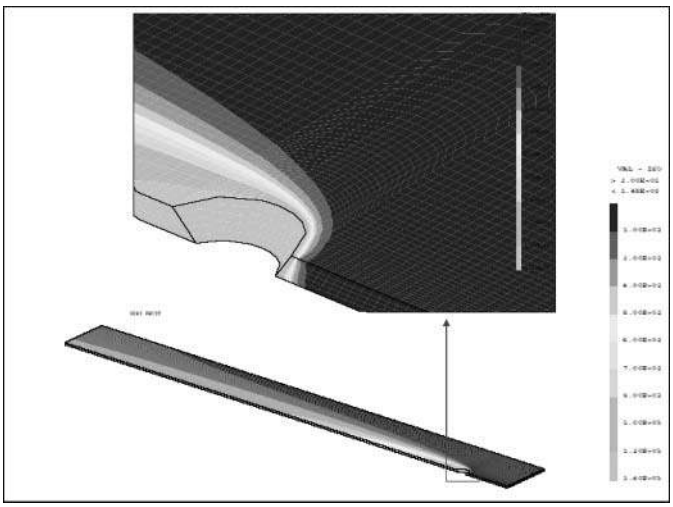

Figure 15 Temperature field within the solid domain.

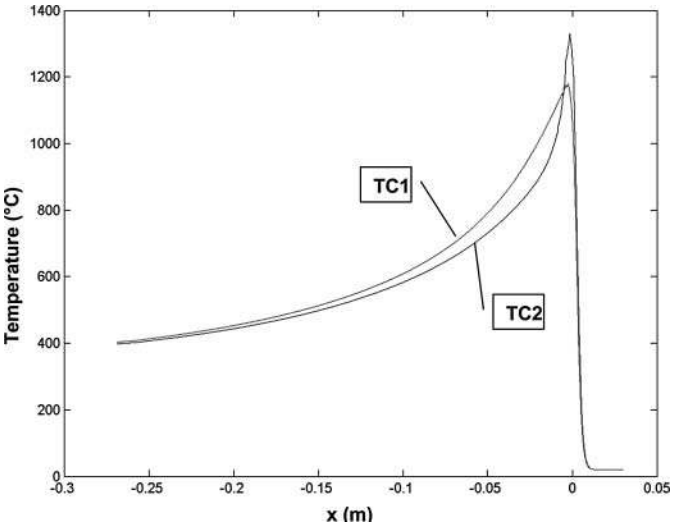

Figure 16 Temperature signals TC1 and TC2.

As in the 2-D case, to facilitate the numerical procedure, we make the parameter coordinates in the range [0, 1] by a simple transformation: $P_{ijk} = \|P_{ijk}\|/\|P_{ijk}^{norm}\|$, $P_{i=0,jk} = \|P_{i=0,jk}\|/0.0065$, $P_{i\neq 0,jk} = \|P_{i\neq 0,jk}\|/0.01$.

The vector parameter transformed to be found is then:

$$X_{tr}^{\exp} = [0.923\,0.615\,0.923\,0.923\,0.750.50.60.90.90.60.81]$$

By applying the initial conditions (B*), we have:

$$P_{23x} = P_{20x} = P_{13x} = P_{10x} = \frac{a}{0.01}$$

$$P_{21y} = P_{22y} = P_{11y} = P_{12y} = \frac{4}{3*0.01}b = \frac{4}{0.03}b$$

$$P_{03x} = P_{00x} = \frac{a}{0.0065}$$

$$P_{01y} = P_{02y} = \frac{4}{3*0.0065}b = \frac{4}{0.0195}b$$

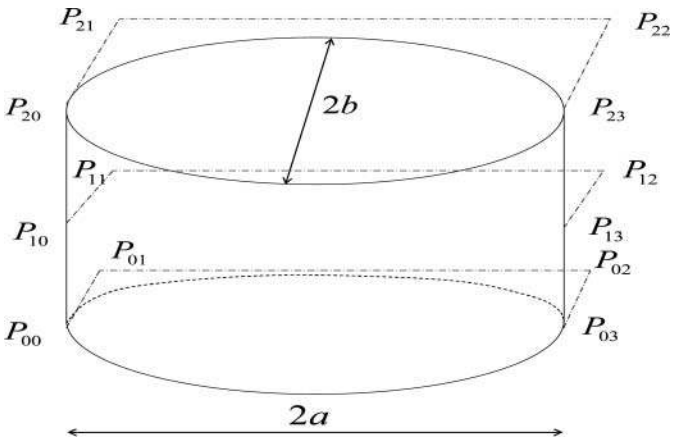

Figure 17 Configuration of the initial parameter choice.

Table 5 Initial parameters

Test number	$X^{ini} = \left[P_{00x}^{ini}, P_{03x}^{ini}, P_{01y}^{ini}, P_{02y}^{ini}, P_{10x}^{ini}, P_{13x}^{ini}, P_{11y}^{ini}, P_{12y}^{ini}, P_{20x}^{ini}, P_{23x}^{ini}, P_{21y}^{ini}, P_{22y}^{ini}\right]$
1	[0.225 0.225 0.1875 0.1875 0.18 0.18 0.15 0.15 0.18 0.18 0.15 0.15]

Table 6 3-D full penetration case result

Test number	$\sqrt{S}$	Iteration number	$\sqrt{S}/T_{\max}$ (%) ($T_{max} = 1331.3°$)	ε^{est} (%)
1	5.32	40	0.4	8.59

$$P_{ijk} \in [0, 1] \text{ then } 0 < a < 0.01; 0 < b < \frac{0.03}{4}$$

Several tests, with various vectors of initial parameters (Table 1), are carried out in order to analyze convergence.

In the test cases presented here, we consider $M = 100$ measurement points, both on the top and on the bottom of the plate. This number of measurement points was found to be a satisfactory compromise between the computing time and the set of data required for an accurate estimation.

We present in Table 5 the initial parameters used with $a = 0.0036; b = 0.00125$, and in Table 6 the optimization problem result.

We present the estimated parameters evolution of this test case in Figures 18 and 19, the comparison between the exact front and the estimated one in Figure 20, and the difference between these two fronts in Figures 21 and 22.

Following the 2-D analysis result, the initial shape (Figure 20) was selected inside the exact form. One observes in Figures 21 and 22 a more important error in estimating the back of welding pool at $x \approx -5mm$. That result should be improved

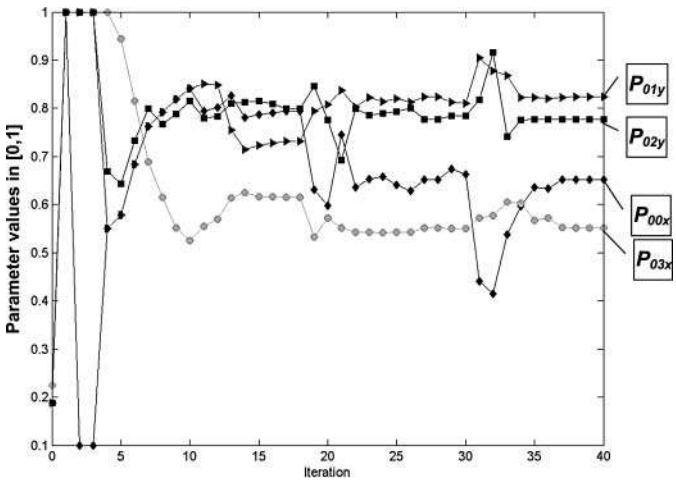

Figure 18 Iterative estimation of parameters P_{00x}, P_{03x}, P_{01y}, P_{02y}.

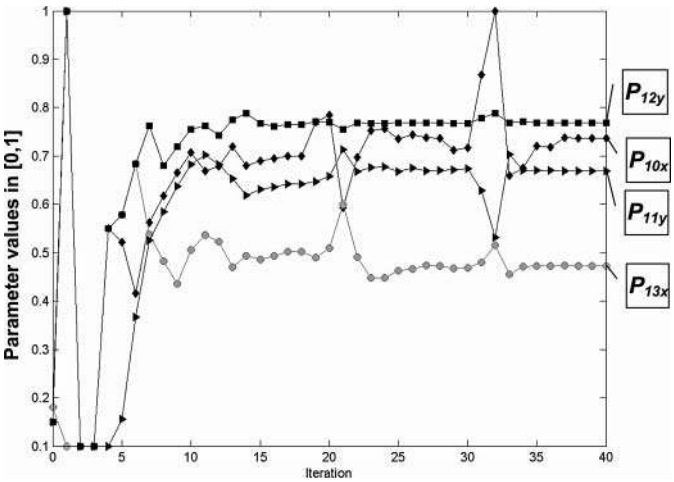

Figure 19 Iterative estimation of parameters P_{10x}, P_{13x}, P_{11y}, P_{12y}.

by lengthening the measurement zone toward the back of the welding pool.

Partial Penetration Case

We present here a case test representative of a TIG or MIG/MAG welding process configuration. The liquid/solid interface (fusion front) is parameterized by using Bezier surface of degree 2×3. Applying the same method of reduction of the parameters number presented previously, the fusion front can be written as (Figure 23):

$$X = [P_{00x}, P_{01x}, P_{01z}, P_{02x}, P_{02z}, P_{03x}, P_{11x},$$

$$\times\ P_{11y}, P_{12x}, P_{12y}, P_{21x}, P_{22y}] \text{ (N = 12)}$$

Numerical Experiment (Figures 24–26). The reference temperature field presented in Figures 27 and 28 is obtained using Cast3M software (Figure 26) with the following data:

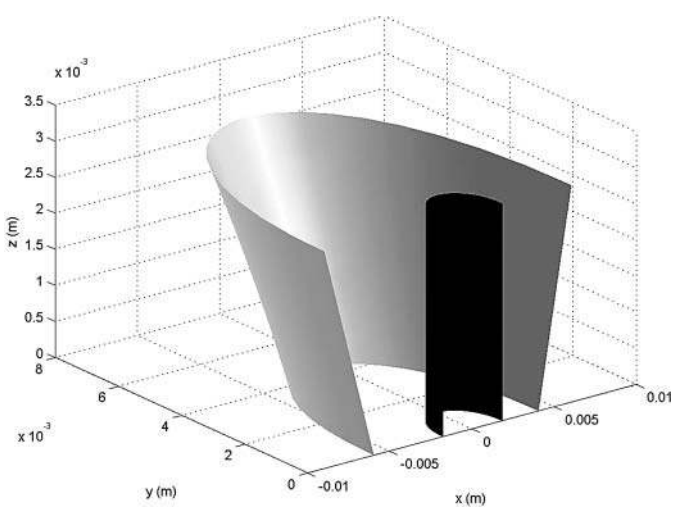

Figure 20 Initial front (black) and exact front (gray).

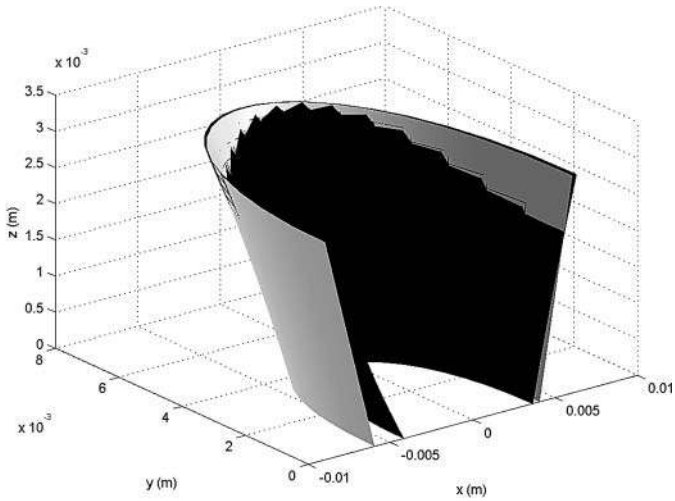

Figure 21 Comparison between the exact front and the estimated one.

$h = 24.1\text{W m}^{-2}\text{ K}^{-1}$, $L_y = 40\ mm$, $L_x = 300\ mm$, $e = 3\ mm$, $\rho_s c_p = 4000000\ J.m^{-3}.K^{-1}$, $\lambda_s = 50\ W.m^{-1}.K^1$, $T_f = 1450°C$, $T_{imp} = 20°C$, and $v_{torche} = 10\,mm.s^{-1}$.

The shape of the front is parameterized by the following 12 control points:

$$P_{00}^{\exp} \equiv P_{10}^{\exp} \equiv P_{20}^{\exp} = (-0.006700)$$
$$P_{01}^{\exp} = (-0.0047\,0\,0.00)$$
$$P_{02}^{\exp} = (0.0013\,0\,0.002)$$
$$P_{03}^{\exp} \equiv P_{13}^{\exp} \equiv P_{23}^{\exp} = (0.0033\,0\,0.008)$$
$$P_{11}^{\exp} = (-0.0047\,0.002\,0.002)$$
$$P_{12}^{\exp} = (0.0013\,0.004\,0.002)$$
$$P_{21}^{\exp} = (-0.0067\,0.005\,0.008)$$
$$P_{22}^{\exp} = (0.0033\,0.008\,0.008)$$

We use two sensors, one located on the top plane ($z = e$) TC1 ($Y_{tc1} = 6\ mm$, $Z_{tc1} = 8\ mm$) and the other one located within the work piece TC2 ($Y_{tc2} = 5\ mm$, $Z_{tc2} = 6\ mm$) (Figure 24).

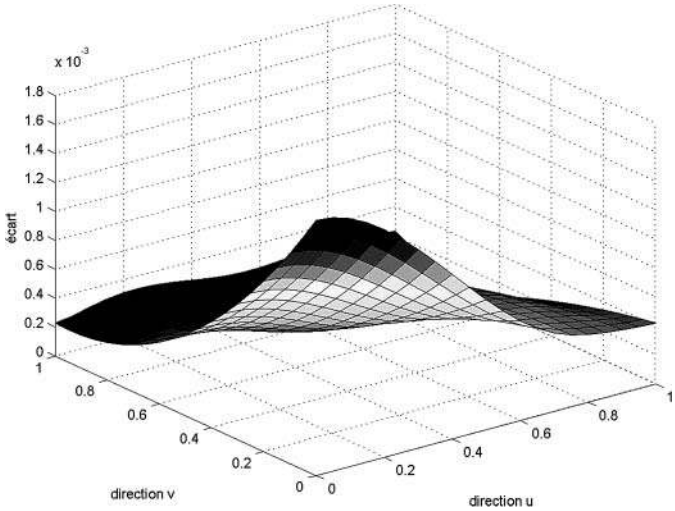

Figure 22 The error between the exact front and the estimated one.

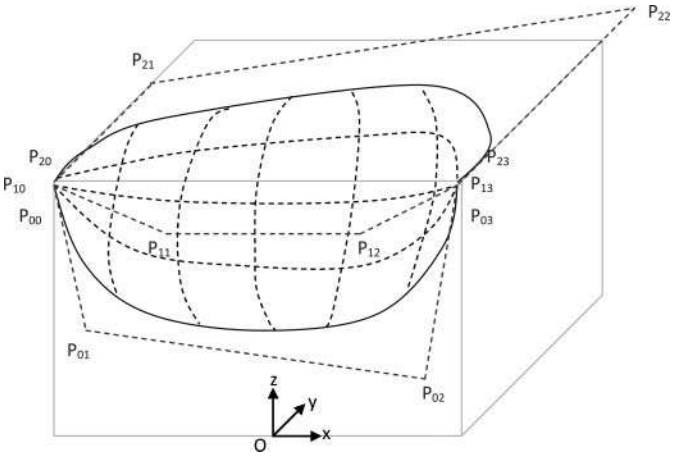

Figure 23 Bezier surface of degree (2 × 3).

Results and Discussion—Influence of the Choice of Initial Parameters X^{ini}. The parameters vector to be identified is:

$$X = \left[P_{00x}, P_{01x}, P_{01z}, P_{02x}, P_{02z}, P_{03x}, P_{11x}, P_{11y}, \times P_{12x}, P_{12y}, P_{21y}, P_{22y}\right]$$

$$X^{\exp} = [-0.0067 - 0.0047 - 0.006\,0.0013 - 0.006\,0.0033 \\ -0.0047\,0.002\,0.0013\,0.004\,0.005\,0.008]$$

We apply the technique already presented in the 3-D full penetration case concerning the choice of the initial values of the parameters: The constraint to be respected is that the weld pool length must be higher or equal to its width. The initial parameters must in addition satisfy the following conditions:

$$\left.\begin{array}{l} P_{23x} = P_{13x} = P_{03x} = a; \quad P_{00x} = P_{10x} = P_{20x} = -a \\ P_{21y} = P_{22y} = \frac{4}{3}b \\ P_{01z} = P_{02z} = \frac{4}{3}c \\ a > b, e > c(\text{e} = \text{platethickness}) \end{array}\right\} (\text{C}^*)$$

This configuration is presented in Figure 28.

Parameter normalization is carried out in order to put them in the interval [0, 1]:

$$P_{00x} = \frac{\|P_{00x}\|}{0.01}, P_{01x} = \frac{\|P_{01x}\|}{0.005}, P_{11x} = \frac{\|P_{11x}\|}{0.005},$$

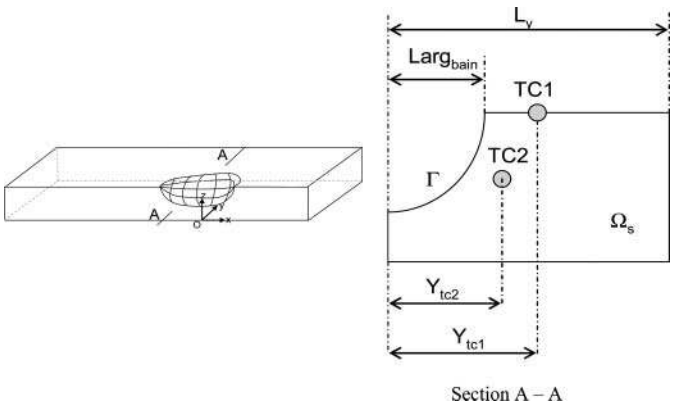

Figure 24 Sensor location in 3-D partial penetration case.

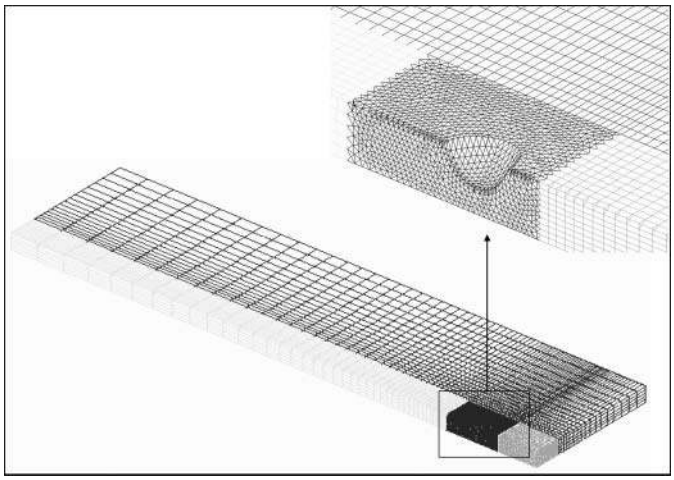

Figure 25 3-D mesh corresponding to partial penetration case.

$$P_{03x} = \frac{\|P_{03x}\|}{0.005}, P_{02x} = \frac{\|P_{02x}\|}{0.005}, P_{12x} = \frac{\|P_{12x}\|}{0.005}$$

$$P_{11y} = \frac{\|P_{11y}\|}{0.005}, P_{12y} = \frac{\|P_{12y}\|}{0.005}, P_{21y} = \frac{\|P_{21y}\|}{0.01},$$

$$P_{22y} = \frac{\|P_{22y}\|}{0.01} P_{01z} = \frac{\|P_{01z}\|}{0.008}, P_{02z} = \frac{\|P_{02z}\|}{0.008}$$

By applying the initial conditions C* we have:

$$P_{23x} = P_{13x} = P_{03x} = \frac{a}{0.005}; P_{00x} = P_{10x} = P_{20x} = \frac{a}{0.01}$$

$$P_{21y} = P_{22y} = \frac{4}{3*0.01}b = \frac{4}{0.03}b;$$

$$P_{11y} = P_{12y} = \frac{4}{3*0.005}b = \frac{4}{0.015}b;$$

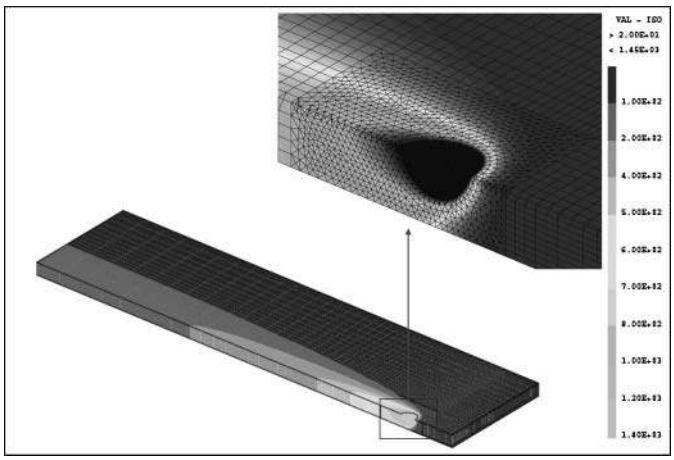

Figure 26 Temperature field within the solid domain.

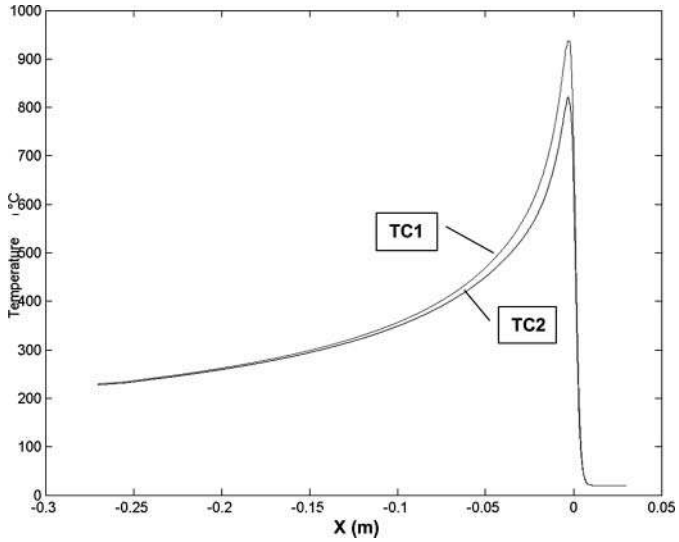

Figure 27 Temperature signals TC1 and TC2.

$$P_{01z} = P_{02z} = \frac{4}{3{*}0.008}c = \frac{4}{0.024}ca > b,$$

$$e > c, 0 < a0.01; 0 < b < \frac{0.015}{4}; 0 < c < 0.006$$

As in the preceding study, we choose a number of measurement points allowing a good compromise between the computing time and the quantity of sufficient information for the estimation: 51 measurement points coming from the temperature signal TC1 and 51 measurement points from TC2 (Figure 24).

Table 7 points out the used initial parameters vector and Table 8 summarizes the estimation results.

Figures 29 to 31 describe the parameters evolution during the estimate. Figure 32 shows a comparison between the exact and estimated fusion fronts. Lastly, the difference between these two fronts is presented in Figure 33.

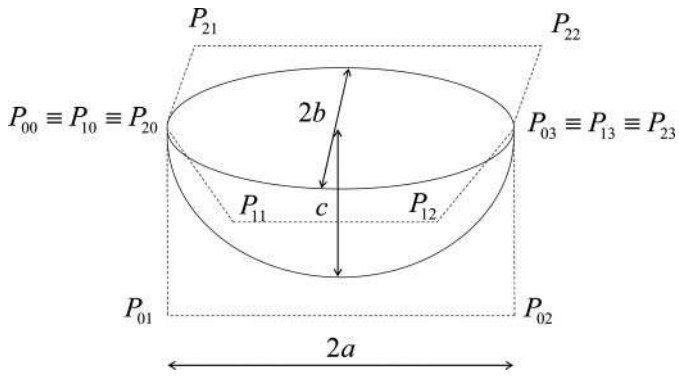

Figure 28 Initial parameter choice configuration.

Table 7 Initial parameters vector

Test number	$X^{ini} = \left[P_{00x}^{ini}, P_{01x}^{ini}, P_{01z}^{ini}, P_{02x}^{ini}, P_{02z}^{ini}, P_{03x}^{ini}, P_{11x}^{ini}, P_{11y}^{ini}, P_{12x}^{ini}, P_{12y}^{ini}, P_{21y}^{ini}, P_{22y}^{ini}\right]$
1	[0.150.30.2250.30.2250.30.30.520.30.520.260.26]

Table 8 Estimation results of a 3-D partial penetration case

Test number	$\sqrt{S}$	Iteration number	$\sqrt{S}/T_{\max}$ (%) ($T_{\max} = 932^{\circ}C$)	ε^{est} (%)
1	8.973	35	0.96	11.92

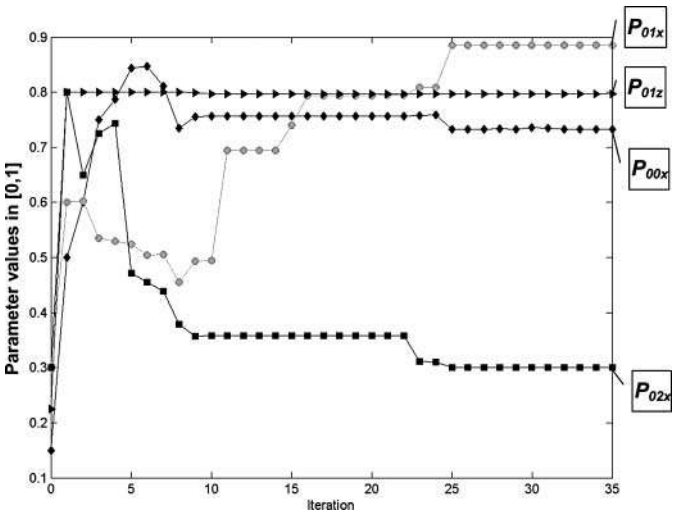

Figure 29 Iterative estimation of parameters P_{00x}, P_{01x}, P_{01z}, P_{02x}.

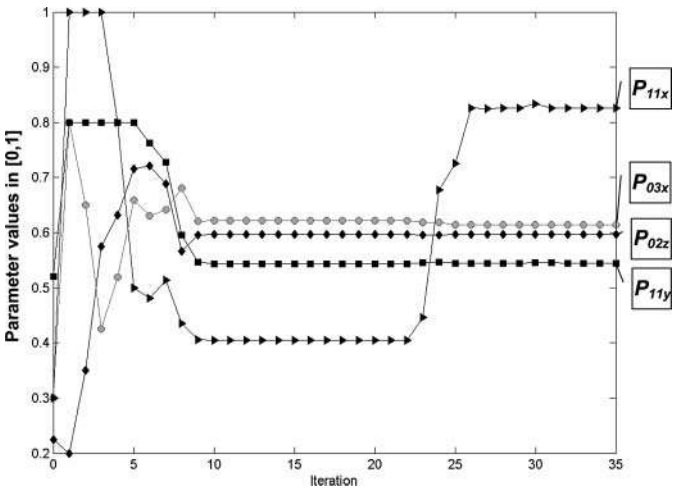

Figure 30 Iterative estimation of parameters P_{02z}, P_{03x}, P_{11x}, P_{11y}.

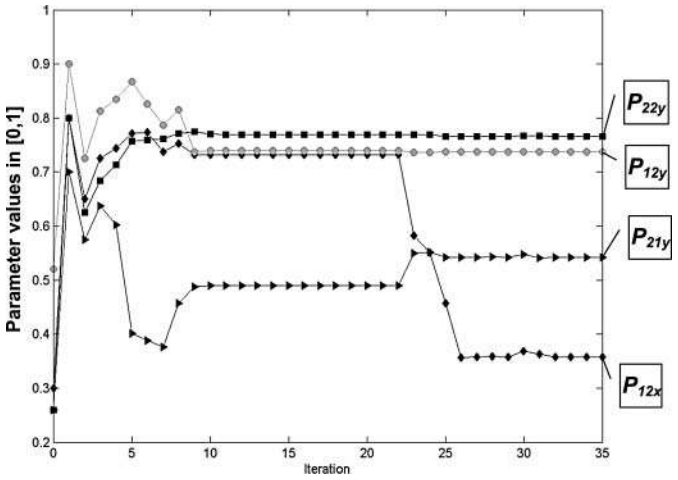

Figure 31 Iterative estimation of parameters P_{02z}, P_{03x}, P_{11x}, P_{11y}.

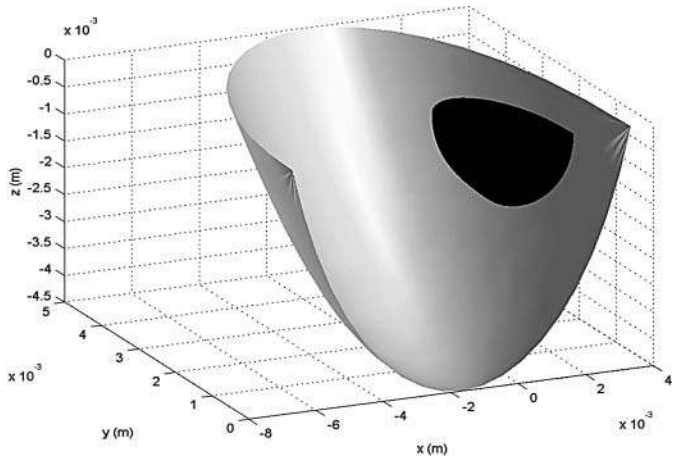

Figure 32 Initial front (black) and exact front (gray).

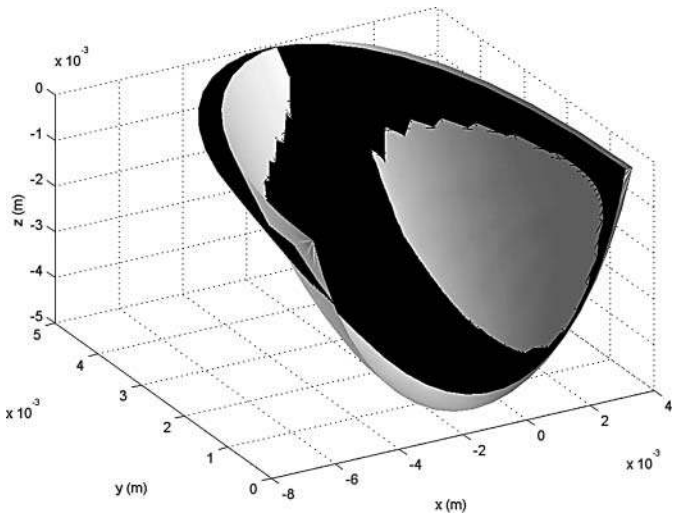

Figure 33 Comparison between the exact and estimated fronts.

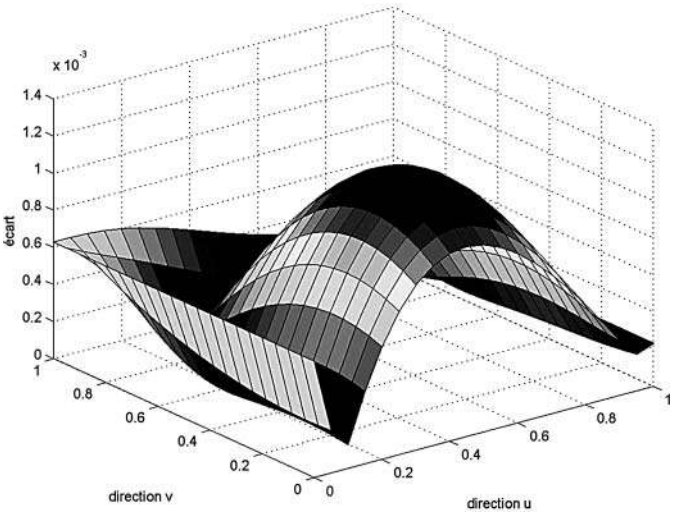

Figure 34 Error between estimated and exact fronts.

In the same way as in the 2-D and 3-D full penetration cases, the initial form (Figure 32) was selected inside the exact form.

One observes in Figures 33 and 34 a more important error in estimating the back of the weld pool shape at $x \approx -7mm$. This result should be corrected by lengthening the zone of measurement toward the back of the weld pool.

CONCLUSIONS

This paper discussed the development and the validation of a numerical method to identify the shape of the phase-change front in a quasi-steady-state welding process. The problem is formulated as an inverse geometry problem and it is solved iteratively by minimizing a standard least-squares criterion. Fast convergence is achieved by modeling the unknown shape of the interface with Bezier surfaces (3-D) or Bezier splines (2-D). The main advantage of this approach is due to the small number of parameter values to be identified, which consequently reduces the amount of required additional measurement data.

It is shown that temperature measurements available only in the solid region of the work piece to be welded are sufficient to estimate the shape of the front, without considering heat transfer and fluid flow in the molten zone, which simplifies considerably the modeling of the welding process. Moreover, after estimation of the shape, the method gives directly the heat flux density that enters into the solid region through this shape. Finally, the method is sufficiently general to be applied to a great variety of welding processes: tungsten inert gas (TIG), metal inert gas (MIG), metal active gas (MAG), laser or electron beam, or hybrid welding processes.

NOMENCLATURE

a, b, c dimensions of the fusion zone
$B_i^m(u)$ Bezier function

$B_j^n(v)$	Bezier function
c	specific heat capacity, J kg^{-1} K^{-1}
C_i^n	Bezier function
e	thickness of the work piece, m
h	overall heat transfer coefficient, W m^{-2} K^{-1}
L_1	dimension behind the fusion zone, m
L_2	dimension in front of the fusion zone, m
L_x L_y	dimensions of the domain, m
m	measurement point
M	number of points of measurement
p	perimeter of the specimen, m
P_{xxx}	parameter of the Bezier surface
P_i, P_{ij}	parameter of the Bezier spline
P(u,v)	function of the Bezier surface
P(t)	function of the Bezier spline
S(T)	objective function
S(Γ)	objective function
S	section of the specimen, m^2
T	temperature, K
T_s	temperature within the solid domain, K
T_e	exterior temperature, K
T_{imp}	imposed temperature, K
T_f	melting temperature, K
u, v	Bezier variables
u	torch velocity, m s^{-1}
x, y, z	spatial variables, m
Y^m	temperature measurement at sensors location, K

Greek Symbols

ε	emissivity of the specimen
ε^{est}	estimation error
λ_s	thermal conductivity of the solid, W m^{-1} K^{-1}
ρ_s	density of the solid, kg m^{-3}
Γ	liquid–solid interface
Ω_s	solid domain

Subscripts

calc	calculated data
est	estimated value
exp	experimental data
l	liquid phase
ref	reference
s	solid phase
TC	thermocouple

REFERENCES

[1] Zacharia, A., David, S., Vitek, J., and Debroy, T., Weld Pool Development During GTA and Laser Beam Welding of Type 304 Stainless Steel, part 11, Experimental Correlation, *Welding Journal*, vol. 68, pp. 510–519, 1989.

[2] Thompson, M., and Szekely J., The Transient Behavior of Weld Pool With A Deformed Free Surface, *International Journal of Heat and Mass Transfer*, vol. 32, pp. 1007–1019, 1989.

[3] Katz, M., and Rubinsky, B., An Inverse Finite Element Technique to Determine the Change of Interface Location in One Dimensional Melting Problem, *Numerical Heat Transfer*, vol. 7, pp. 269–283, 1984.

[4] Zabaras, N., and Ruan, Y., A Deforming Finite Element Method Analysis of Inverse Stefan Problem, *International Journal of Numerical Methods in Engineering*, vol. 28, pp. 295–313, 1989.

[5] Rubinsky, B., and Shitser, A., Analytic Solution to the Heat Equation Involving a Moving Boundary With Application to the Change of Phase Problem: The Inverse Stefan Problem, *ASME Journal of Heat Transfer*, vol. 100, pp. 300–304, 1978.

[6] Hsu, Y. F., Rubinsky, B., and Mahin, K., An Inverse Finite Element Method for Analysis of Stationary Arc Welding Processes, *Journal of Heat Transfer*, vol. 108, pp. 734–741, 1986.

[7] Al-Khadily, N., Application of Optimisation Methods For Solving Inverse Phase-Change Problems, *Numerical Heat Transfer, B*, vol. 31, pp. 477–497, 1997.

[8] Zabaras, N., and Yuan, K., Dynamic Programming Approach to the Inverse Stefan Design Problem, *Numerical Heat Transfer*, vol. 26, pp. 97–107, 1994.

[9] Nowak, I., Nowak, A. J., and Wrobel, L. C., Identification of Phase Change Fronts by Bezier Splines and BEM, *International Journal of Thermal Science*, vol. 41, 492–499, 2002.

[10] Doan, D. D., Gabriel, F., Jarny, Y., and Le Masson, P., Utilisation des courbes de Bezier pour l'identification du front de fusion dans une opération de soudage, *in Proceeding of the Congrès Français de Thermique, SFT 2006*, Ile de Ré, 16/05/2006-19/05/2006, France.

[11] Lewis, R. W., Morgan, K., Thomas, H. R., and Seetharamu, K. N., *The Finite Element Method in Heat Transfer Analysis*, Wiley, Chichester, 1996.

[12] Zerrokat, M., Power, H., and Wrobel, L. C., Heat and Solute Diffusion With a Moving Interface: A Boundary Element Approach, *International Journal of Heat and Mass Transfer*, vol. 41, pp. 2429–2436, 1998.

[13] Doan, D. D., Gabriel, F., Jarny, Y., and Le Masson, P., Identification of a Phase Change Front by Bezier Splines for the Heat Transfer Analysis of Welding Processes, *MCWASP, Opio, France*, 2006.

[14] Doan, D. D., *Thesis, Modèle de source de chaleur pour la simulation du soudage avec et sans apport de matière*, University of Nantes, France, October, 2006.

[15] Özisik, M. N., and Orlande, H., *Inverse Heat Transfer Fundamentals and Applications*, Taylor & Francis, New York, 2000.

[16] Goldak, J., Bibby, M, Moore, J., House, R., and Patel, B., A New Finite Element Model for Welding Heat Source, *Metallic Transactions B*, vol. 15B, pp. 299–305, 1984.

Duc Dung Doan is a research engineer at Hong Bang Group (HBG) in Viet Nam. Prior to joining HBG, he worked as a postdoctoral research associate at Institut de Radioprotection et de Sûreté Nucléaire (IRSN) in France. He received his Ph.D. in mechanics and thermics from University of Nantes in 2006. He has a patent with the Energy Atomic Agency in France and several articles concerning the new method to identify the weld pool shape by using Bezier surface developed during his thesis. Now, he leads a small team in HBG Science Division in the mechanics field.

Franck Gabriel is a senior research engineer at the Commissariat à l'Energie Atomique, Saclay, France, in the reactor studies and applied mathematics section. He received his Ph.D. in heat and mass transfer engineering from Nantes University in 1996. His research interests include material processing modeling, heat and mass transfer modeling, and system engineering particularly applied to thermonuclear fusion reactor components and technologies.

Yvon Jarny has a doctor-ès-sciences (1987) and is a professor at Polytech'Nantes, the Engineering School of the University of Nantes. His research interests include modeling and control of heat transfer, thermal characterization of polymer and composite materials, optimal control of forming processes, and theory and practice of inverse heat transfer problems. He has coauthored 140 refereed journal publications and conference proceedings, and has contributed to several books. He served as director of the Thermal and Energy Sciences Department of Polytech'Nantes. He is a fellow of the SFT (Societé Française de Thermique) and leader of the French group METTI (Metrologie Thermique et Techniques Inverses). He serves on the editorial board of *IPSE.* He is currently working on the homogenization theory of composite structures, and the heat transfer modeling in the injection molding process.

Philippe Le Masson has a doctor-ès-sciences (1991) and is a Professor at the University of South Brittany of Lorient. He works in the Laboratory LIMATb. His research interests includes modeling of heat transfer, theory and practice of inverse heat transfer problems, measurements with thermocouples, and thermal characterizations of the heat transfer during process. He is a director of the Energy Sciences Department of the University of South Brittany. He is a member of the SFT (Société Française de Thermique) and works in the French group METTI (Metrologie Thermique et Techniques Inverses). He works more specially on the modeling (fluid mechanics, interaction process–material) and the instrumentation by thermocouples of welding operations.